Authors' preprint of:
S.L. Sheehe and S.I. Jackson. "Identification of species from visible and near-infrared spectral emission of a nitromethane-air diffusion flame." Journal of Molecular Spectroscopy, Vol. 364, pp. 1111 85, 2019.
https://doi.org/10.1016/j.jms.2019.111185

Identification of Species from Visible and Near-Infrared Spectral Emission of a Nitromethane-Air Diffusion Flame

Suzanne L. Sheehe[1] and Scott I. Jackson

Los Alamos National Laboratory, NM 87545, USA

Abstract

The combustion processes of nitromethane, an explosive used in many combustion applications, are not fully captured in current state-of-the-art nitromethane kinetic schemes. There is a need for data on transient species to further improve understanding of nitromethane chemistry and dynamics. This work aims to identify transient species present during nitromethane-air combustion through characterization of the spectral emission of a flame stabilized on an aluminum oxide wick at atmospheric pressure. Assignments were made using a spectral library assembled from prior literature and through comparison with spectra taken in two additional air-diffusion flames, CD_3NO_2 and CH_3OH. Several new emitters were detected in excited electronic states: HNO*(A'), CN* ($A^2\Sigma$), NO_2*, and in ground electronic states: CH, OH, NH, and H_2O. The previously observed reaction species CH*($A^2\Delta$) was also observed, while formaldehyde and the characteristic C_2*($A^3\Pi_g$) Swan bands were not.

Keywords

Nitromethane, diffusion flame, emission spectroscopy, flame structure, UV-VIS spectroscopy

1. Introduction

[1] Corresponding author. *Email address:* ssheehe@lanl.gov

Nitromethane has long been of interest to the combustion community due to its applicability as a fuel in automobiles and as a monopropellant [1-10]. As the simplest fuel containing a nitro group, it serves as an excellent model material for more complex energetic materials for interrogation of the mutual sensitized oxidation of hydrocarbons and nitrogen oxides [1-10]. For example, current understanding of RDX combustion is heavily reliant on nitromethane studies [1].

Prior works highlight the need for additional data to improve understanding of nitromethane chemistry. For example, the initiation step for nitromethane combustion is not well understood. Historically, the initiation step for nitromethane combustion was largely accepted as decomposition to CH_3 and NO_2 with subsequent reactions involving transient species and intermediates [11-20]. Recently, some reaction schemes have included an initiation step with a branching reaction where CH_3NO_2 undergoes rearrangement to CH_3ONO^* with rapid decomposition to CH_3O and NO [7,9, 11, 21-22]. In addition, validation studies compared predictions from the most recent proposed mechanisms (Brequigny et al 2015 [4] and Mathieu et al 2016 [7]) to experiment and found deviations with shock tube ignition, flame structure, laminar burning velocity, and flame height measurements [5-10].

Improved understanding of nitromethane chemistry in deflagrations requires (1) increased characterization of the chemical flame structure and (2) identification, characterization and improved understanding of the relevance of excited state species in the reaction kinetics (as existing mechanisms generally only include ground state species). Emission spectroscopy measurements are able to address both needs by identifying species present at

various flame locations from analysis of their spectral emissions. These emitters are highly dependent on local compositions and can therefore be used to identify local ground state species and associated pathways [23-32].

Emission spectroscopy in the ultra violet-visible (UV-VIS) region (200-450 nm) has been successfully applied to various nitromethane flame geometries. In these studies, the flame was observed to have an inner flame core attributed to self-sustained combustion and an outer shell supported by air [12, 15-16]. At lower pressure, 10 kPa, nitromethane-air and nitromethane-oxygen flames exhibited an orange broadband continuous broadband emission in the inner zone and the following emitters in the outer shell: $C_2^*(A^3\Pi_g)$, $CH^*(A^2\Delta)$, $CN^*(B^2\Sigma)$, $OH^*(A^2\Sigma^+)$, $NH^*(A^3\Pi)$, and $NO^*(A^2\Sigma)$ [20]. All of these species were also observed in nitromethane pool fire flames at both atmospheric and higher pressures, except for the $C_2^*(A^3\Pi_g)$ Swan bands and $CH^*(A^2\Delta)$ [14-15]. Formaldehyde emission has been observed in shock tube studies, but was not detected in any of these flames [33-34].

In this work, we characterized nitromethane flame emission in the visible and near-infrared (VIS-NIR) regime (400 – 975 nm) and associated the observed spectral emitters with specific molecules using prior work and theory. A low-resolution broad-spectrum spectrometer was chosen for these initial studies to enable single shot capture of a broad number of emitting species. The laminar diffusion flame was stabilized on a cylindrical aluminum oxide wick. The stable flame allowed time-averaged measurements at a well-defined spatial resolution and emission spectra were taken as a function of flame height and radial position. This data was used to identify transient emitting species in the nitromethane flame by comparison with

literature and with spectra taken in two additional diffusion flames using the same flame configuration, perdeutero nitromethane (CD_3NO_2) and methanol (CH_3OH).

2. Experimental Method

The experimental assembly consisted of a liquid candle enclosed in a flame cell with optical fiber access as shown in the schematic of Fig. 1. The liquid candle was composed of a wick held in a brass holder and partially submerged in a test tube containing the fuel (Fig. 1). The wick was a cylindrical piece of fibrous aluminum oxide with a 6.0 mm ± 0.5 mm diameter machined from a Buster-M35 ceramic insulation board (Zircar Zirconia, New York). This fibrous aluminum oxide had a capillary network consisting of pressed micro-fibers that act to pull fuel from the test tube via surface tension. The wick was mounted in the top of the test tube by a brass ring with a set screw. The bottom of the wick was submerged into the 35-cm^3 test tube containing the fuel. Three fuels were studied: (i) nitromethane, (Acros Organic, 99+% for analysis), (ii) perdeutero-nitromethane, (CD_3NO_2, Aldrich, 99% atom D), and (iii) methanol (CH_3OH, Fisher Chemical, Acetone free, Absolute). The oxidizer-diluent mixture was atmospheric air at ambient pressure, which is approximately at 0.766 atm (77.6 kPa) at the test facility location.

Authors' preprint of:
S.L. Sheehe and S.I. Jackson. "Identification of species from visible and near-infrared spectral emission of a nitromethane-air diffusion flame." Journal of Molecular Spectroscopy, Vol. 364, pp. 1111 85, 2019.
https://doi.org/10.1016/j.jms.2019.111185

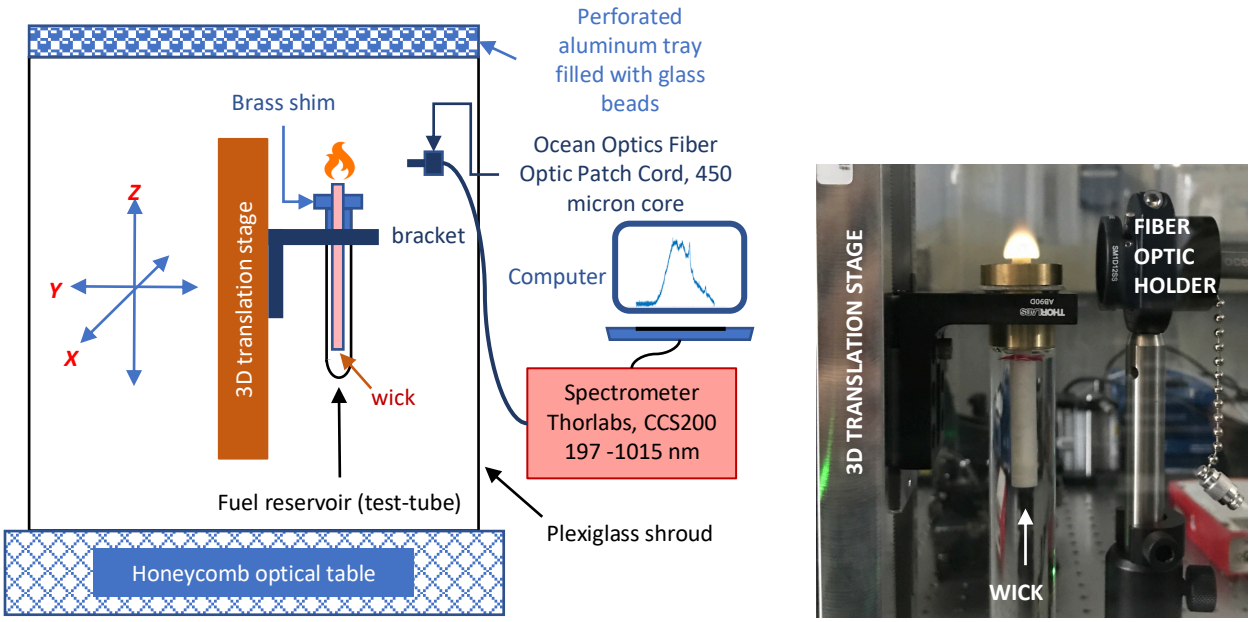

Fig. 1. a) Schematic of experiment and b) framing camera image of experiment

The flame was located in a flame cell enclosure to ensure a laminar and steady burn. The enclosure integrated plexiglass sidewalls with a porous top and bottom. The bottom was fabricated from a perforated steel sheet and backed by a sintered metal filter. The top was a perforated aluminum tray filled with glass beads. The sidewalls contained feedthrough ports for optical access. To further ensure a steady flame, the test tube was refilled and the wick surface cleaned after every three minutes of use, which was the typical acquisition time for a single averaged spectrum. Cleaning the wick prevented the accumulation of soot, which could block portions of the capillary channels and result in flow instabilities. This accumulation was difficult to see with the naked eye and it only takes a few small soot particles in a capillary to cause instabilities. Note that smoke was not visibly observed for both the nitromethane and

perdeutero-nitromethane flames. It is expected that contributions from incandescent emission of soot will either be negligible or not observed.

Figure 2 shows two perspectives of the nitromethane flame, which measured approximately 12 mm in diameter and 8 mm in height. The flame appeared semi-transparent (Fib. 2b) and orange-yellow to the naked eye (Fig. 1b). The flame was lifted and slightly wrapped around the wick (Fig. 2a). Optical flame transparency is further discussed in [35].

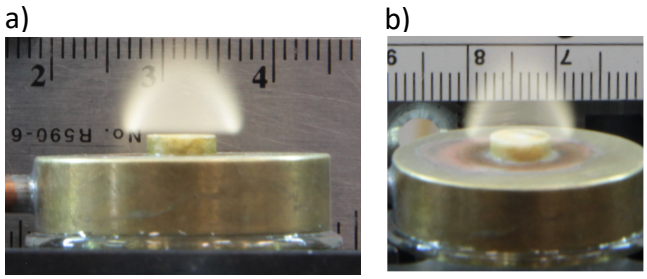

Fig. 2. Two views of the nitromethane-air diffusion flame stabilized on the wick: a) metal ruler in background and b) white ruler in background

Flame emission was measured with a fixed optical fiber that was located 11.9 $\pm$ 0.5 mm from the wick centerline (z-axis in Fig. 1). The flame and test tube were translated vertically (z-axis) and horizontally (x-axis) with a three-axis translation stage (Velmex Inc. New York), with resolution of 0.25 mm. The optical fiber was a 1-m long Ocean Optics solarization resistant SMA patch cord optical fiber that was transparent from 200-1100 nm with a core of 450 ± 8 microns and a numerical aperture of 0.2. The fiber connected to a (Thorlabs CCS200) low-resolution Czerny-Turner spectrometer with a 20 µm by 1.2 mm entrance slit, 600 lines/mm grating, and a 3648-pixel CCD line array with a FWHM spectral resolution of approximately 1.5 nm. Collected spectra were averaged over three minutes with individual spectrum integration times in the range 4 – 15 s. Emission spectra were taken at 8 different flame heights (along the

z-axis) and various radii (along the x-axis) to yield 69 total spectra per experiment. Spectra were corrected for dark current and system response (wavelength and intensity). Spectral analysis using the corrected spectra is discussed in section 3.

The spectrometer was calibrated using emission from fiber coupled neon, argon, and zinc lamps (Avantes, AvaLight-CAL-Neon-Mini, AvaLight-CAL-Argon-Mini, AvaLight-CAL-Zinc). The calibration was then verified against flame emission of Na and CaOH, generated by sprinkling NaCl and CaCl2 (Aldrich, 99.99%)) salts onto the wick prior to ignition. The resulting calibration was found to be accurate to within $\pm$ 0.4 nm of literature values [36]. Spectral intensity was also calibrated with two NIST-traceable lamps, a 200-W-quartz-halogen-tungsten-filament lamp with output 3280 K (Oriel Part# 63355) and a deuterium lamp (Ocean Optics, DH-3plus) by averaging dark and light spectra over six minute intervals. A 10% discrepancy was found between the two lamp calibrations.

3.0. Results and Discussion

3.1. Centerline spectra and summary of analysis

Figure 3 shows centerline spectra of the nitromethane diffusion flame from six flame heights above the wick surface with spectral assignments for the most intense bands. These spectra show characteristic bands for CH*($A^2\Delta$), HNO*(A^1A''), CN*($A^2\Pi$), NO_2*, CH, OH, NH, H_2O, and Na* (a contaminant). Observation of these emitters in deflagrating nitromethane are novel to this work. While ground state HNO has previously been detected [1], this is the first measurement of HNO* emission in nitromethane flames. These transitions of CH, OH, NH, and H_2O have also not been previously observed in a nitromethane flame because this is the

first study to examine emission in the VIS-NIR region. The characteristic C_2* swan bands are not observed. This is consistent with observations in flames with fuels containing NO_2 functional groups or NO_2 additives with pressures at ~7.3 kPa (50 torr) and higher [15, 37-40].

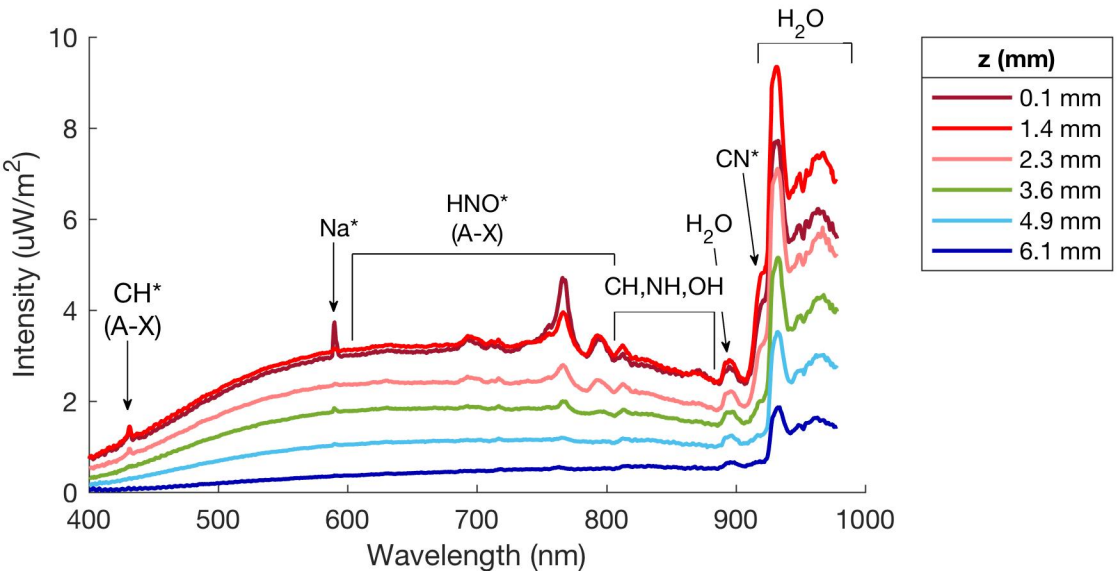

Fig. 3. Corrected emission spectra taken at various flame heights along the centerline of the nitromethane diffusion flame with spectral assignments.

These assignments were determined through comparison of band position and shape with literature, theory, and experimental perdeutero-nitromethane flame emission spectra (see Fig. 4). The identified bands derive from electronic transitions (denoted by *) or ground electronic state vibrational-rotational transitions. The assignments and their literature comparisons for each identified molecule in Fig. 3 are detailed in Table 1.

Authors' preprint of:
S.L. Sheehe and S.I. Jackson. "Identification of species from visible and near-infrared spectral emission of a nitromethane-air diffusion flame." Journal of Molecular Spectroscopy, Vol. 364, pp. 1111 85, 2019.
https://doi.org/10.1016/j.jms.2019.111185

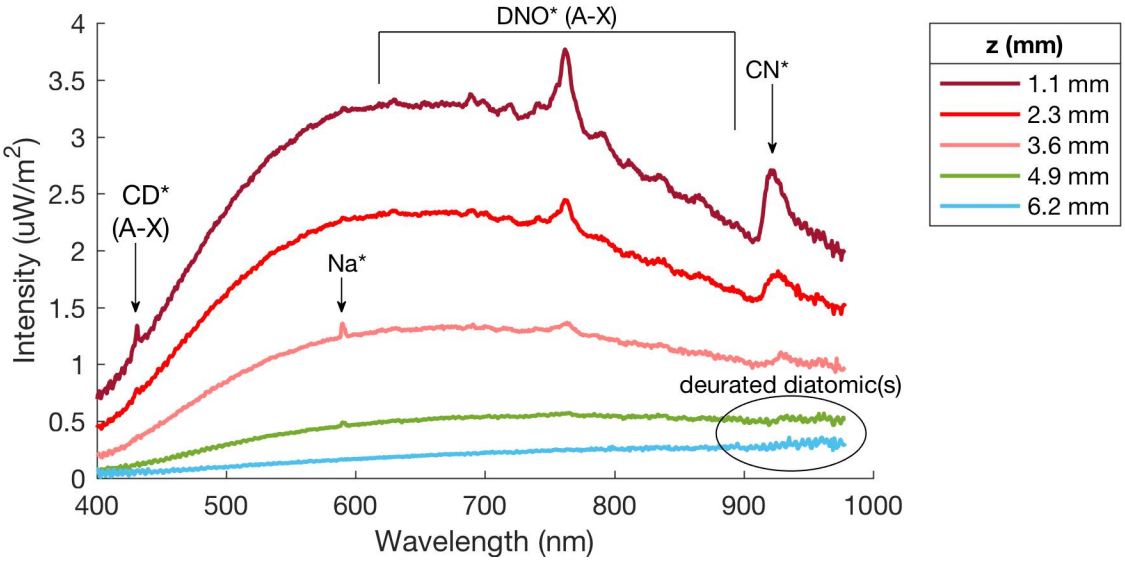

Fig. 4. Corrected emission spectra taken at various flame heights along the centerline of the perdeutero-nitromethane (CD_3NO_2) diffusion flame with spectral assignments.

Table 1: Assignments and features for identified emitters in nitromethane diffusion flames. Intensity notation, vs, s, m, w, and vw, are qualitative descriptors to indicate very strong, strong, medium, weak and very weak maxima

Peak Maxima (this work) ±0.4 nm	*Intensity (this work)*	*Peak positions in literature*	*Assignment (this work)*
CH* emission			
431.4 nm	s	431.4 nm [36]	Q-head $A\ ^2\Delta(0) \rightarrow X\ ^2\Pi\ (0)$
Na* emission			
589.4 nm	s s	589.0 nm [41] 589.6 nm [41]	Na (I) $3p_{3/2} \rightarrow 3s_{1/2}$ Na (I) $3p_{1/2} \rightarrow 3s_{1/2}$
HNO* emission			
868.7 – 871.8	w	879.5 ± 4.6 nm [42] 865.0 ± 8.0 nm [43]	$A^1A''(000) \rightarrow X^1A'(010)$
Peak Maxima (this work) ±0.4 nm	*Intensity (this work)*	*Peak positions in literature*	*Assignment (this work)*
HNO* emission continued			
793 – 797.2	m	796.5 ± 7.0 nm [43]	$A^1A''(100) \rightarrow X^1A'(100)$
763.3 – 766.6	vs	766.3 ± 3.5 nm [42] 760.2 nm [44] 762.6 ± 1.0 nm [43]	$A^1A''(000) \rightarrow X^1A'(000)$

716.3	w	716.2 nm [43]	$R_{K'=13\rightarrow K"=12}$ $\mathrm{A^1A''(000)\rightarrow X^1A'(000)}$
710.4 – 711.3	w	707.5 nm [44] 710.0 ± 3.0 nm [43]	$\mathrm{A^1A''(001)\rightarrow X^1A'(000)}$
692.8	m	693.5 ± 2.5 nm [42] 692.5 ± 6.0 nm [43]	$\mathrm{A^1A''(020)\rightarrow X^1A'(010)}$
687.6	w	686.1 nm [44]	$\mathrm{A^1A''(010)\rightarrow X^1A'(000)}$
677.6	vw	677.3 nm [44] 677.1 nm [43]	$R_{K'=4\rightarrow K"=3}$ $\mathrm{A^1A''(010)\rightarrow X^1A'(000)}$
671.7	vw	671.7 nm [44] 671.7 nm [43]	$R_{K'=6\rightarrow K"=5}$ $\mathrm{A^1A''(010)\rightarrow X^1A'(000)}$
668.5	vw	668.6 nm [43]	$R_{K'=7\rightarrow K"=6}$ $\mathrm{A^1A''(010)\rightarrow X^1A'(000)}$
662.9	vw	662.8 nm [43]	$R_{K'=9\rightarrow K"=8}$ $\mathrm{A^1A''(010)\rightarrow X^1A'(000)}$
629.6 – 633.6	vw	627.2 ± 5.0 nm [43]]	$\mathrm{A^1A''(020)\rightarrow X^1A'(000)}$
CH vibrational-rotational emission			
812.7 nm	s	812.95 nm [41, 45] 812.96 nm [41, 45]	$P_{5\rightarrow 0}(3)$ $P_{6\rightarrow 0}(23)$
827.6	m	827.58 nm [41, 45] 827.68 nm [41, 45] 827.69 nm [41, 45]	$Q_{6\rightarrow 0}(27)$ $R_{9\rightarrow 2}(30)$ ‡ $R_{9\rightarrow 3}(12)$
847.3	w	847.19 nm [41, 45] 847.34 nm [41, 45]	$R_{5\rightarrow 0}(11)$ $P_{5\rightarrow 0}(21)$
Peak Maxima (this work) ±0.4 nm	*Intensity (this work)*	*Peak positions in literature*	*Assignment (this work)*
NH vibrational-rotational emission			
828.8	m	828.79 nm [41, 45] 828.82 nm [41, 45] 828.83 nm[41, 45]	$Q_{7\rightarrow 2}(11)$ $R_{7\rightarrow 2}(15)$ $P_{9\rightarrow 3}(17)$
836.7	m	836.73 nm [41, 45]	$Q_{5\rightarrow 0}(25)$

‡ Unlikely transition because the head of this vibrational transition when deuterated is still within range of the spectrometer at ~850 nm. See section A.4 for more detail.

838.1	m	838.01 nm [41, 45]	$Q_{10\rightarrow4}(13)$
844.0	w	844.08 nm [41, 45]	$R_{6\rightarrow1}(24)$
OH vibrational-rotational emission			
835.2 nm	m	834.92 nm [36, 41, 45, 46] 835.16 nm [36, 41, 45, 46] 835.43 nm [36, 41, 45, 46]	$R_{6\rightarrow2}(3)$ $R_{6\rightarrow2}(5)$ $R_{6\rightarrow2}(6)$
842.1 nm	m	841.89 nm [36, 41, 45, 46] 841.90 nm [36, 41, 45, 46] 841.99 nm [36, 41, 45, 46] 842.18 nm [36, 41, 45, 46] 842.25 nm [36, 41, 45, 46] 842.28 nm [36, 41, 45, 46]	$P_{5\rightarrow1}(11)$ $Q_{5\rightarrow1}(15)$ $Q_{5\rightarrow1}(2)$ $R_{6\rightarrow2}(10)$ $Q_{6\rightarrow2}(15)$ $Q_{10\rightarrow5}(2)$
845.0	w	844.78 nm [36, 41, 45, 46] 844.92 nm [36, 41, 45, 46] 845.21 nm [36, 41, 45, 46]	$Q_{5\rightarrow0}(4)$ $P_{5\rightarrow0}(3)$ $R_{5\rightarrow0}(8)$
H_2O vibrational-rotational emission			
Band centered at 895 nm	s	891.6 nm [36]	Overlapping vibrational-rotational bands (see [72] for list of bands)
Band maxima from ~928 – 980 nm	vs	927.7 nm [36] 933.3 nm [36] 944.0 nm [36] 948.5 nm [36] 955.9 nm [36] 961.1 nm [36] 966.9 nm [36] 966.9 nm [36]	Overlapping vibrational-rotational bands (see [72] for list of bands)
CN* emission			
Shoulder at ~ 917 nm	s	916.8 (R-branch) [36] 918.9 (Q-branch) [36]	R- and Q- branches $A^2\Pi(1) \rightarrow X^2\Sigma(0)$
Peak Maxima (this work) $\pm$0.4 nm	*Intensity (this work)*	*Peak positions in literature*	*Assignment (this work)*
NO_2* emission			
Broadband emission from ~400 nm to NIR		From approximately 380 nm to the near infrared (1000 nm) [47-53]	$A^2B_2 \rightarrow X^2A_1$ $B^2B_1 \rightarrow X^2A_1$

			$a^2A_2 \rightarrow \mathrm{X}^2A_1$ †

3.2. CH ($\mathrm{A}\ ^2\Delta$) emission*

The emission spectra show a strong violet degraded peak at 431.4 nm characteristic of the CH* ($\mathrm{A}\ ^2\Delta - \mathrm{X}\ ^2\Pi$) emission band (see Fig. 3) [36]. This is confirmed by a blue shift to 431.0 nm upon deuteration (perdeutero-nitromethane flame, see Fig. 4). The literature value for CD* emission is 430.8 nm [36], which is within the experimental uncertainty of the wavelength calibration of 431.0 nm.

3.3. Na emission*

Sodium emits a doublet at 589.0 and 589.6 nm [36, 41]. A strong line is observed at 589.4 nm and expected to result from the convolution of the two lines due to the coarse spectral resolution. The assignment was confirmed by sprinkling a small amount of NaCl onto the wick and observing a corresponding increase in emission intensity at 589.4 nm.

3.4. HNO emission*

The bands in the region 650-900 nm have been attributed to HNO* emission. As can be observed in Table 1 and Fig. 3, HNO* emission is complex with different vibrational bands, as well as different K sub-bands within the vibrational bands, of the $\mathrm{A}^1\mathrm{A}'' \rightarrow \mathrm{X}^1\mathrm{A}'$ electronic transition [42-44, 54-57]. This complexity results from a bent molecular geometry that is considered a near prolate top with C_2 symmetry in both the excited and ground state. Consequently, there are two "good" quantum numbers, J and K, that describe the angular

† This is a tentative assignment because this transition is spin forbidden. It is possible that this transition may be partially allowed due to vibronic interactions or intersystem crossing with the B_2 or B_1 states [50], but this has not been proven conclusively as of yet.

momentum (rotational energies): (i) J is the value of the total angular momentum, and (ii) K is the absolute value of the angular momentum projected along the symmetry axis for the limiting prolate top [36]. Therefore, the transitions in Table 1 have the vibrational transition $(v_1v_2v_3)'$-$(v_1v_2v_3)''$ and, as assigned previously in the literature, also the sub-band K'-K'' designation. The three vibrational modes are the N-H stretch (v_1), the N=O stretch (v_2), and the bend (v_3). Note that the peak observed at 796 nm has been assigned to the H-N stretch (100)-(100), following the suggestion in [41]. In [58, 59], this band was instead assigned to the bending motion (001)-(001), but the reasons for the assignment change were not discussed.

Peak maxima for some HNO* bands are reported as a range in Table 1 because the peak maxima shift with flame height. The literature values fall within these ranges. For example, the (000)-(000) band shifts from ~ 766.2 to ~ 763.3 nm with increasing z-position, as shown in Fig. 5. This shift indicates changing population distribution among the K sub-bands (K'=3 to K'=1) and could be indicative of changing temperature [36, 42].

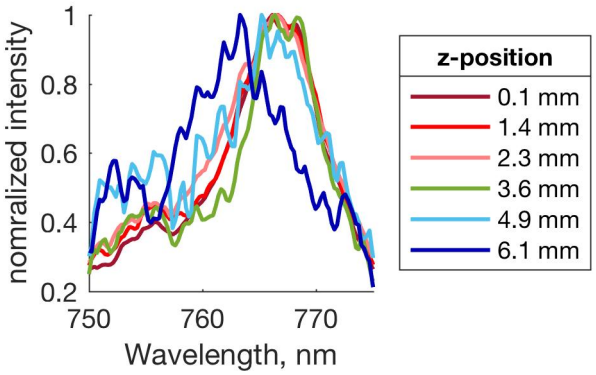

Fig. 5. HNO* (000)-(000) emission band for various z-positions in nitromethane diffusion flame. Spectra are corrected for background, continuous emission, and detector response (intensity).

The HNO* assignments were confirmed by deuterated nitromethane (DNO) spectra as seen in Fig. 6. Observed bands seen in Fig. 6 agree well with literature description of DNO* bands [43], as described in Table 2 .

Table 2: DNO* assignments and features

Peak maxima (this work) ±0.4 nm	*Intensity (this work)*	*Peak Positions in Clement and Ramsay (1961) [39]*	*Assignment (this work)*
873.7	vw	871.15 ± 3.0 nm	(010)-(020)
833.8	w	834.5 ± 3.0 nm	(010)-(100)
811.0	w	810.0 ± 2.0 nm	(000)-(001)
789.6	m	782.0 ± 5.0 nm	(100)-(100)
761.9	vs	759.5 ± 6.0 nm	(000)-(000)
720.0	m	720.0 ± 2.5 nm	(001)-(000)
Peak maxima (this work) ±0.4 nm	*Intensity (this work)*	*Peak Positions in Clement and Ramsay (1961) [39][43]*	*Assignment (this work)*
698.4	w	697.0 ± 2.0 nm	(020)-(010)
688.5	m	687.5 ± 2.0 nm	(010)-(000)
652.7	vw	652.5 ± 2.0 nm	(011)-(000)
630.1	w	629.1 ± 2.0 nm	(020)-(000)

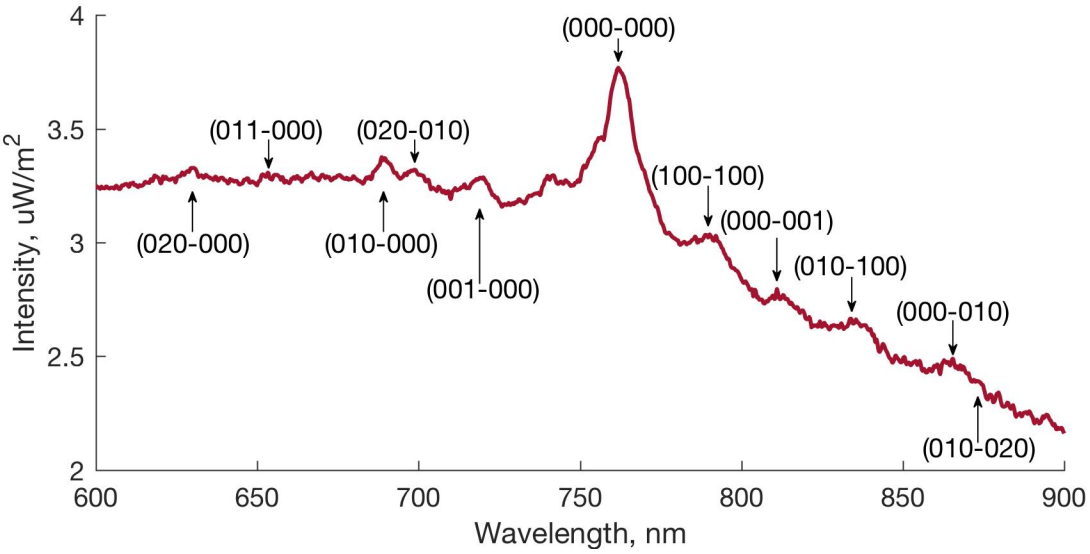

Fig. 6. Typical emission spectrum collected in CD_3NO_2 diffusion flames at 1.1 mm above the wick surface. The spectrum is intensity and background corrected. DNO peak assignments are shown in arrows.

3.5. Vibrational emission in ground electronic states for heterogenous diatomics, CH, OH, and NH.

In the region from 806-863 nm, there exists an open envelope spanning nearly 100 nm. Such a broad open structure is typical of vibrational-rotational transitions of hydrogen containing diatomics [36, 45]; other diatomics, like CN, NO, or CO, have a rotational constant that is an order of magnitude smaller than hydrogen containing diatomics, which results in a more spectrally compact structure due to decreased spacing between rotational lines [41, 45]. Given that the fuel is nitromethane, it is likely that the hydrogen containing diatomic is one of, or a mixture of, the following species: CH, NH, and OH.

The species present in the band(s) for each z-position were determined by comparison of experimental peak position with theoretical peak positions of CH, NH, and OH. The theoretical peak positions were calculated using a Dunham potential for an oscillator with 30 rotational levels and 10 vibrational levels [45]. Only P, Q, and R branches were considered. The requisite diatomic constants for CH, NH, and OH were obtained from the NIST webbook [41]. The calculated peak positions for OH were compared against the HITRAN database [46] and the difference between the two was less than 0.1 cm^{-1}, giving confidence that theoretical peak positions are well within experimental uncertainty. Comparison between theory and experiment show that, at each z-position, there is no single diatomic that can be assigned to the open-envelope structure. Multiple peaks within the structure could be any of the three species

due to the inadequate resolution of the spectrometer. Yet, a few peaks are partially isolated and can be attributed to a single diatomic species and these are listed in Table 1.

The perdeutero-nitromethane flames show no corresponding structure (e.g., extremely open envelope) in the emission spectra. Possible explanations include: (i) the deuteration has red-shifted the peaks out of the range of the spectrometer or (ii) the deuterated flame temperature is too low to excite the vibrational modes. It is unlikely to be the latter because a methanol flame also exhibits the same open envelope as shown in Fig. 7 and the methanol flame is known to be cooler than a nitromethane flame with lower adiabatic flame temperatures [16,62]. Thus, the former is the more likely explanation. This means that, of the vibrational transitions in listed in Table 1 for each isolated peak, the lower v' excitations are more likely in the methanol flames (indicated in Table 1).

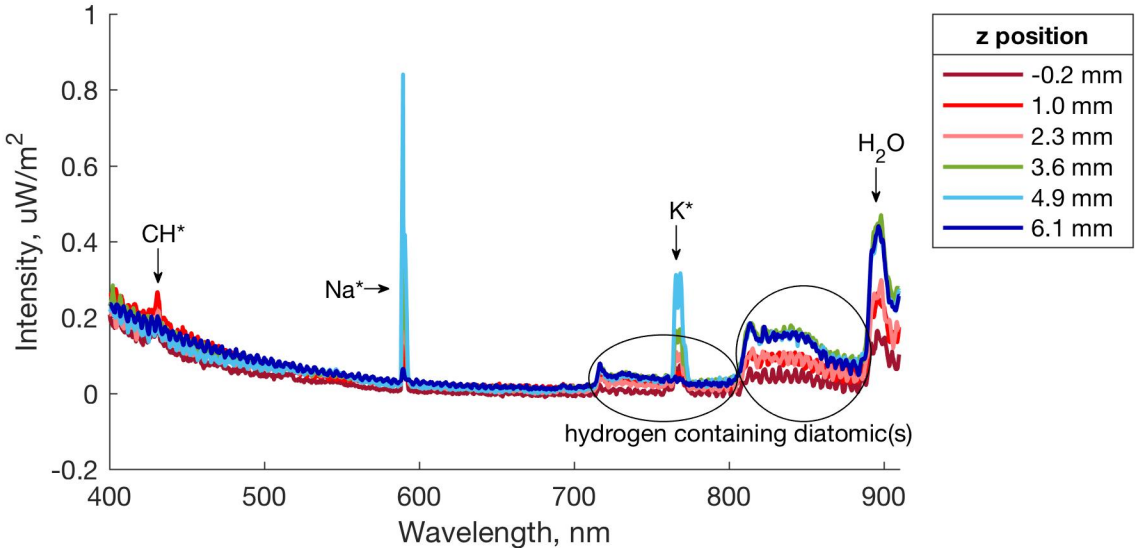

Fig. 7. Typical emission spectrum collected along the centerline in CH_3OH diffusion flames at various z-positions. The spectrum is intensity and background corrected. Peak assignments are shown.

As shown in Fig. 7, the methanol emission spectra exhibit two bands with wide open envelopes and heads at 716.5 nm and 813.6 nm which support the assignments in Table 1. The 813.6 nm band head is comparable to the observed band in the nitromethane emission spectra at 812.7 nm (as previously discussed), further confirming the assignments in Table 1. The 716.5 nm has no comparable observed band in the nitromethane emission spectra. Instead, the observed nitromethane emission band at 716.3 nm is assigned to the HNO* emission rather than hydrogen containing diatomics (see Table 1). The HNO* assignment is likely correct for one main reason: the qualitative shape of the band in question is narrower and exhibits a denser structure relative to that observed in the methanol spectra. The narrowness and closed-structure are consistent with HNO* emission (see plates in [44]) suggesting that HNO* emission is dominating this region in nitromethane emission spectra. Another nearby band in the nitromethane emission spectra has a head at 692.6 nm, exhibits similar structure to the band at 716.3 nm, and matches literature values for HNO* emission, providing additional support that the assignment at 716.3 nm is indeed HNO* emission.

Also shown in the methanol spectra in Fig. 7 is a well-defined doublet at 766.2 and 769.7 nm. The two peaks are well resolved and are consistent with K* emission, which has a doublet at 766.5 and 770.0 nm and is a common contaminant [36]. This doublet is not observed in the nitromethane or perdeutero-nitromethane emission spectra where the bands in the 760-770 nm do not exhibit the well-defined doublet structure and also show peak maxima shifting with flame height (reflecting temperature changes). If there is any K* emission in the nitromethane or perdeutero-nitromethane spectra, it would be hidden in the HNO* or DNO* bands which are

an order of magnitude stronger in intensity relative to the K* emission observed in the methanol spectra.

3.6. Vibrational emission in electronic ground states H_2O

The nitromethane flame emission spectra show a band centered around 891.3 nm and series of bands in the region 927-980 nm with sharp intensity maxima characteristic of water vibrational-rotational bands [36, 46]. The band at 891.3 nm is also observed in the methanol emission spectra, see Fig. 7. This assignment is confirmed by the perdeutero-nitromethane flame spectra, shown in Fig. 4, which show no water emission bands. This is expected because deuteration red-shifts the water bands to wavelengths longer than 1000 nm which is outside the spectrometer range [46]. The lack of water bands in the perdeutero-nitromethane flame emission also indicates that the detected emission was not due to thermally excited ambient water and is therefore from combustion products.

3.7. CN emission*

The shoulder on the 927 nm water band at ~917 nm is assigned to CN* emission (see Table 1). This is not an obvious assignment because there are two weak HNO* bands (010-100) and (000-002), with origins near 912 nm [36, 43]. The perdeutero-nitromethane flame spectra clearly show that CN* emission is dominant in this region because Fig. 8a shows that the shoulder at ~917 nm retains the same peak location in perdeutero-nitromethane spectra. Figure 8b also shows the CN* vibrational branches on top of a weak band with open structure due to emission from diatomic CD/OD/ND peaks.

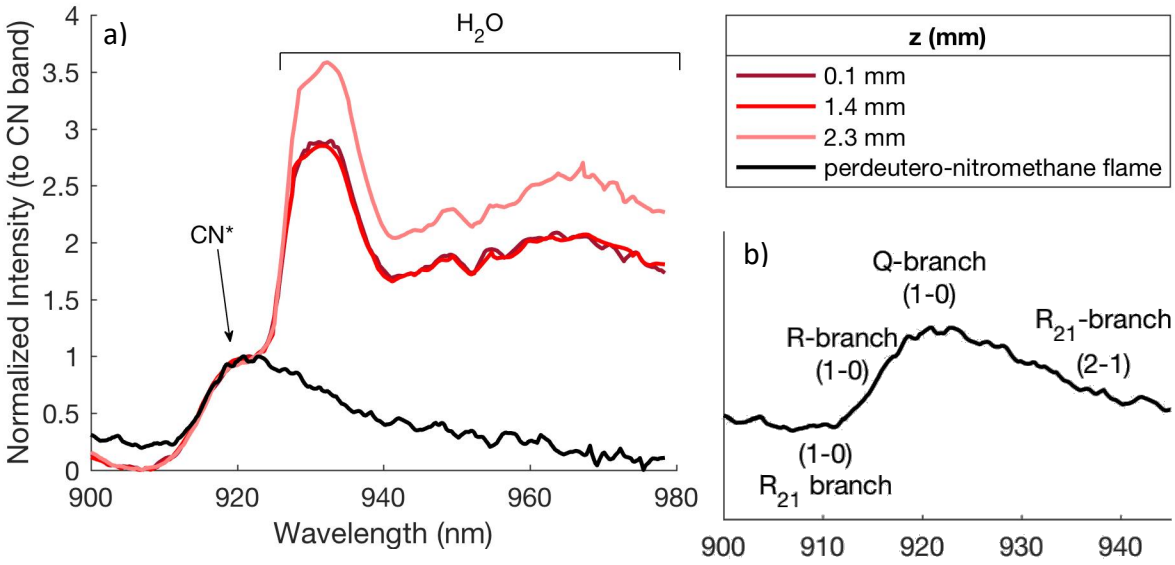

Fig. 8. Emission spectra from nitromethane and perdeutero-nitromethane (CD_3NO_2) diffusion flames: a) comparison of perdeutero-nitromethane flame spectrum with spectra taken at three flame heights (z) in nitromethane flame, and b) perdeutero-nitromethane spectrum with CN* assignments. Spectra have been background and intensity normalized to CN* band. Continuous emission from NO_2 has not been subtracted out.

3.8. NO_2 emission and potential incandescent soot emission*

The emission spectra typically show a broad continuous emission from ~ 400 nm to the near IR that agrees very well with the literature spectrum of NO_2* chemical and thermal emission [47-51]. This close agreement is demonstrated in Fig. 9 where experimental NO_2 emission from [47] is compared with spectra from the centerlines of the CH_3NO_2 and CD_3NO_2 flames. The intensities of the emission curve from [47] and from the CD_3NO_2 have been rescaled so as to match the intensity of the CH_3NO_2 flame. A baseline has also been added to the emission curve from [47] to match that of the present work. Note that the authors in [47] attribute the observed emission to the chemiluminescent reaction which resulted after the

introduction of NO gas and a mixture of O + O_2 gas (partially dissociated upstream in a microwave discharge) into a gas cell at low pressure, ~1-5 torr:

$$O + NO \rightleftharpoons NO_2 + hv \quad (1)$$

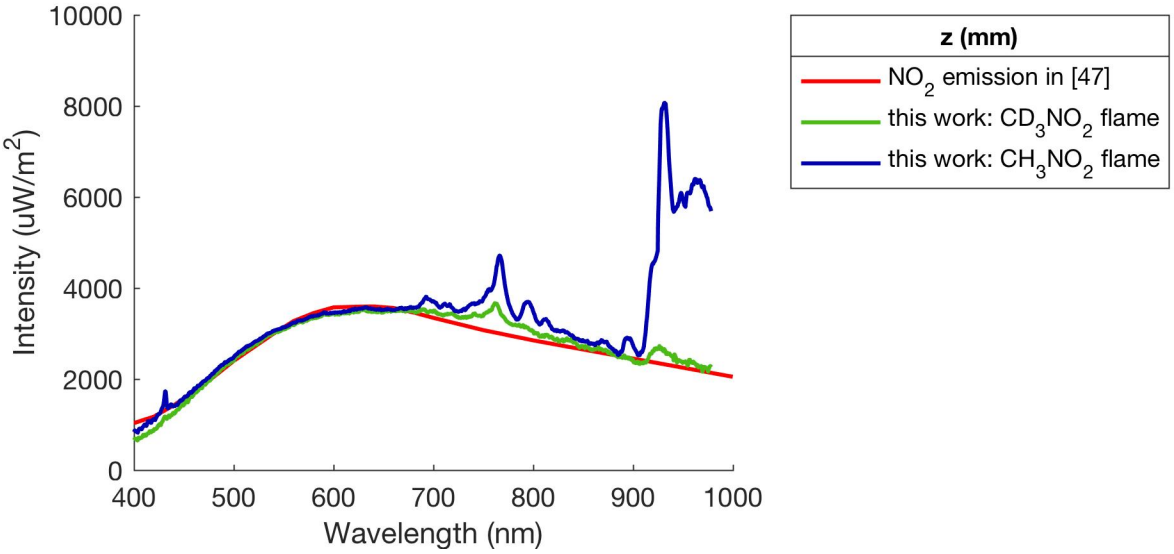

Fig. 9. Comparison of emission from reference [47] (light-blue curve) with emission from the centerline of (i) CH_3NO_2-air diffusion flame at z=0.1 mm (dark blue curve) and (ii) CD_3NO_2-air diffusion flame at z=1.1 mm (blue-green curve).

It is unlikely that the broadband unstructured emission observed in the nitromethane and perdeutero-nitromethane flames is due to incandescent emission soot, which is typically gray body emission. As previously stated, the nitromethane and perdeutero-nitromethane flames are visibly low-sooting. In addition, gray body emission has a very different curvature than what is observed in the present work, as shown in Fig. 10.

Authors' preprint of:
S.L. Sheehe and S.I. Jackson. "Identification of species from visible and near-infrared spectral emission of a nitromethane-air diffusion flame." Journal of Molecular Spectroscopy, Vol. 364, pp. 1111 85, 2019.
https://doi.org/10.1016/j.jms.2019.111185

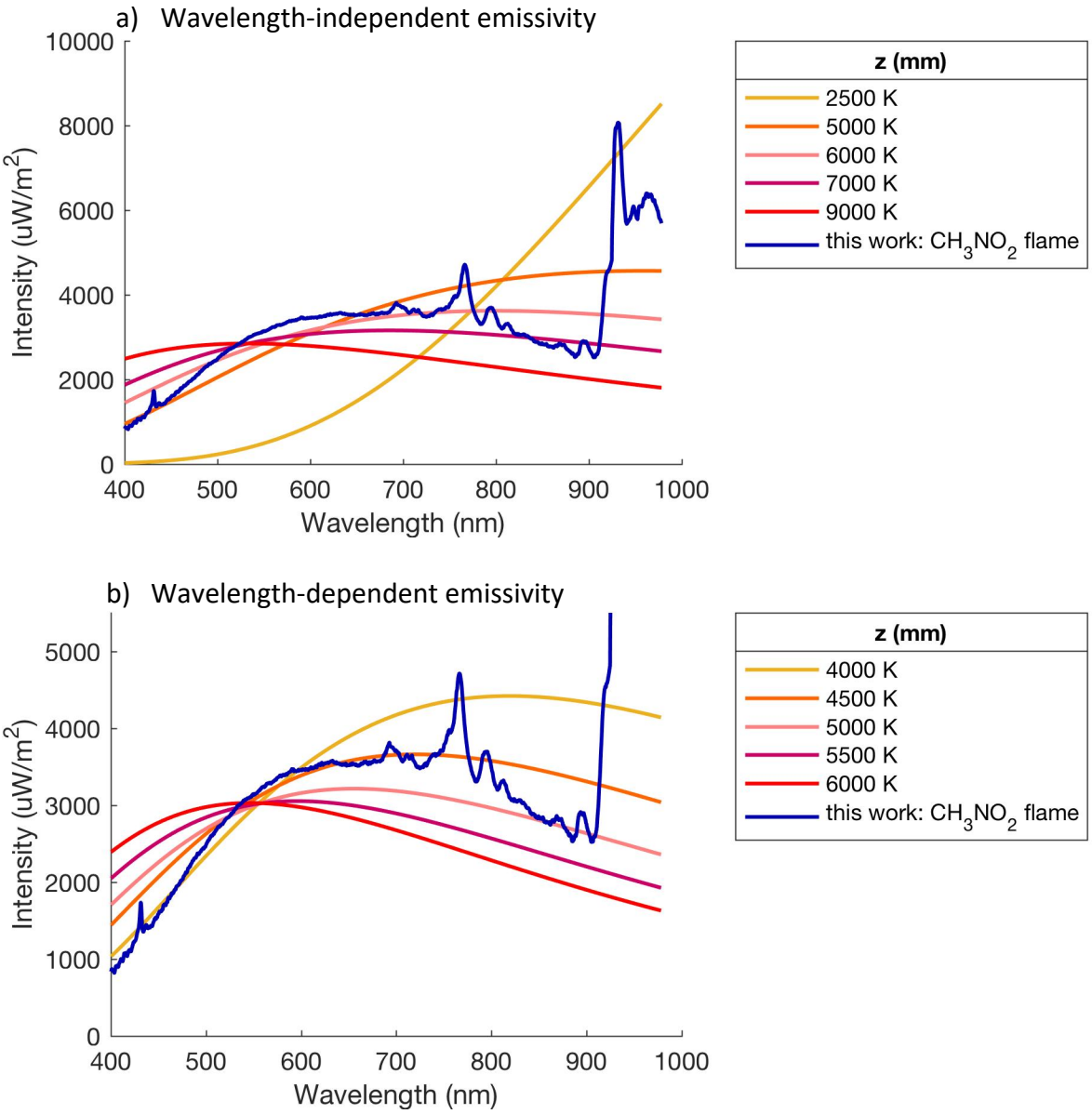

Fig. 10. Graybody emission for five different temperatures were fit to experimental data from the centerline of the CH_3NO_2 flame (z = 0. 1 mm) (dark blue line): a) wavelength-independent emissivity coefficient, and b) wavelength-dependent emissivity coefficient

To generate the gray body curves in Fig. 10, the distribution function for blackbody radiation [45] is modified by multiplication of an emissivity coefficient. For Fig. 10 (a), the emissivity coefficient is wavelength -independent as in [63] and in (b) the coefficient is wavelength dependent as in [64]. Both gray body functional forms for various temperatures

were fitted to the experimental data with the spectral bands removed using a non-linear least squares algorithm in MatLab. As can be seen in Fig. 10, temperatures in excess of 2000 K agree best with the experimental temperature whereas flame temperatures are expected to be around 1500-3000 K [15].

It is likely that NO_2* emission is observed from the multiple electronic transitions indicated in Table 1 because the gray body emission curves clearly have different spectral shapes than that of the experimental data whereas the NO_2 emission from [47] matches the experimental curves well. The NO_2* emission spectra are typically broadband and very complex due to four low-lying states, X^2A_1 A^2B_2, a^2A_2, B^2B_1, that share conical intersections and allow for both intersystem crossing and vibronic interactions [47-51, 65-66]. Therefore, an electronically forbidden transition can be made possible via these mechanisms and adds to the number of possible transitions [48, 65]. The broadness in the observed spectra indicates both chemical and thermal emission from a minimum of three transitions, (i) $\mathrm{A}^2B_2 \rightarrow \mathrm{X}^2A_1$, (ii) $B^2B_1 \rightarrow \mathrm{X}^2A_1$, and (iii) $a^2A_2 \rightarrow \mathrm{X}^2A_1$ [48]. Note that the broadness of the emission does not necessarily indicate a broad internal energy distribution in chemically formed NO_2* (e.g, forming in A^2B_2, B^2B_1, and a^2A_2 electronic states), but could mean emission from a narrow internal energy distribution to multiple lower states. For example, NO_2* could form in the B^2B_1 state and undergo an internal conversion to A^2B_2 before emitting. Therefore, it is not possible to say with certainty from the experimental emission if the chemically formed NO_2* is formed in one electronic state or all three excited electronic states (A^2B_2, B^2B_1, a^2A_2). This uncertainty is why multiple transitions for NO_2 emission are listed in Table 1.

5.0 Summary and Conclusions

In this study, spatially resolved emission spectra were recorded and analyzed from a nitromethane-air diffusion flame stabilized on an aluminum oxide wick. The following emitters were identified in the spectra using information from prior work and theory: CH*($A^2\Delta$), HNO*(A^1A''), CN*($A^2\Pi$), NO_2*, CH, OH, NH, and H_2O. Emission spectra from perdeutero-nitromethane (CD_3NO_2) diffusion flames and methanol (CH_3OH) diffusion flames were used to confirm spectral assignments. Due to a lack of prior measurements in this regime, this is the first report for a nitromethane flame of all of the identified species except CH*($A^2\Delta$), which has been observed previously.

Acknowledgements

We thank Dr. David Moore for helpful discussion regarding spectral assignments.

References

[1] Z.Y. Tian, L.D. Zhang, Y.Y. Li, T. Yuan, F. Qi, An experimental and kinetic modeling study of a premixed nitromethane flame at low pressure, Proc. Combust. Inst. 32 (2009) 311-318.

[2] K.W. Zhang, Y.Y. Li, T. Yuan, J.H. Cai, P. Glarborg, F. Qi, An experimental and kinetic modeling study of premixed nitromethane flames at low pressure, Proc. Combust. Inst. 33 (2011) 407-414.

[3] K. Zhang, L. Zhang, M. Xie, L. Ye, F. Zhang, P. Glarbog, F. Qi, An experimental and kinetic modeling study of premixed nitroethane flames at low pressure, Proc. Combust. Inst. 34 (2013) 617-624.

[4] P. Brequigny, G. Dayma, F. Halter, C. Mounaim-Rousselle, T. Dubois, P. Dagaut, Laminar burning velocities of premixed nitromethane/air flames: an experimental and kinetic modeling study, Proc. Combust. Inst. 35 (2015) 703-710.

[5] J.D. Nauclér, E.J.K. Nilsson, A.A. Konnov, Laminar burning velocity of nitromethane plus air flames: a comparison of flat and spherical flames, Combust. Flame 162 (10) (2015) 3803-3809.

[6] J.D. Nauclér, Y. Li, E.J.K. Nilsson, H.J. Curran, A.A. Konnov, An experimental and modeling study of nitromethane + O_2 + N_2 ignition in a shock tube. Fuel 186 (2016) 629-638.

[7] O. Mathieu, B. Giri, A.R. Agard, T.N. Adams, J.D. Mertens, E.L. Petersen, Nitromethane ignition behind reflected shock waves: experimental and numerical study, Fuel 182 (2016) 597-612.

[8] O. Mathieu, C. Mulvihill, and E.L. Petersen, Experimental study of nitromethane oxidation: CO and H_2O time-histories behind reflected shock waves, 911, 26th ICDERS, IDERS, Boston, MA, USA, July 30th – August 4th, 2017, paper.

[9] C. Brackmann, J.D. Nauclér, S. El-Busaidy, A. Hosseinia, P.E. Bengtsson, A.A. Konnov, E.J.K. Nilsson, Experimental studies of nitromethane flames and evaluation of kinetic mechanisms, Combust. Flame 190 (2018) 327-336.

[10] M. Faghih, Z. Chen, Two-stage heat release in nitromethane/air flame and its impact on laminar flame speed measurement, Combust. Flame 183 (2017) 157-165.

[11] C.J. Annesley, J.B. Randazzo, S.J. Klippenstein, L.B. Harding, A.W. Jasper, Y. Georgievskii, B. Ruscic, R.S. Tranter, Thermal dissociation and roaming isomerization of nitromethane: experiment and theory, J. Phys. Chem. A. 119 (28) (2015) 7872-7893.

[12] A.R. Hall, H.G. Wolfhard, Multiple reaction zones in low pressure flames with ethyl and methyl nitrate, methyl nitrite and nitromethane, Symp. (Int.) Combust. 6 (1957) 190-199.

[13] H.N. Presles, P. Vidal, J.C. Gois, B.A. Khasainov, B.S. Ermolaev, Influence of glass microballoons size on the detonation of nitromethane based mixtures, Shock Waves 4 (6) (1995) 325-329.

[14] H.N. Presles, D. Desbordes, M. Guirard, C. Guerraud, Gaseous nitromethane and nitromethane-oxygen mixtures: a new detonation structure, Shock Waves 6 (2) (1996) 111-114.

[15] W. Eckl, V. Weiser, M. Weindel, N. Eisenreich, Spectroscopic investigation of nitromethane flames, Propellants, Explosives, Pyrotechnics 22 (1997) 180-183.

[16] S. Kelzenberg, N. Eisenreich, W. Eckl, V. Weiser, Modelling nitromethane combustion, Propellants, Explosives, Pyrotechnics 24 (1999) 189-194.

[17] M.O. Sturtzer, N. Lamoureux, C. Matignon, D. Desbordes, H.N. Presles, On the origin of the double cellular structure of the detonation in gaseous nitromethane and its mixtures with oxygen, Shock Waves 14 (1-2) (2005) 45-51.

[18] E. Boyer, K.K. 2007, Modeling of nitromethane flame structure and burning behavior, Proc. Combust. Inst. 31 (2007) 2045-2053.

[19] F. Joubert, D. Desbordes, H.N. Presles, Detonation cellular structure in NO_2/N_2O_4-fuel gaseous mixtures, Combust. Flame 152 (4) (2008) 482-495.

[20] B. Khasainov, F. Virot, H.N. Presles, D. Desbordes, Parametric study of double cellular detonation structure, Shock Waves 23 (3) (2013) 213-220.

[21] P.A. Vlasov, N.M. Kuznetsov, Y.P. Petrov, S.V. Turetskii, Nitromethane isomerization during its thermal decay, Kinet. Catal. 59 (1) 6-10.

[22] A. Matsugi, H. Shiina, Thermal decomposition of nitromethane and reaction between CH_3 and NO_2, J. Phys. Chem. A 121 (22) (2017) 4218-4224.

[23] T. Edwards, D.P. Weaver, D.H. Campbell, S. Husizer, Investigation of high pressure solid propellant combustion using emission spectroscopy, J. Propulsion 2 (3) (1986) 228 -234.

[24] J. Grebe, K.H. Homann, Blue-green chemiluminescence in the system C_2H_2/O/H. Formation of the emitters CH($A^2\Delta$), $C_2(d^3\Pi_g)$, and C_2H^*, Ber. Bunsenges. Phys. Chem. 86 (1982) 587-597.

[25] V.N. Nori, J. M. Seitzman, CH* chemiluminescence modeling for combustion diagnostics, Proc. Combust. Inst. 32 (2009) 895-903.

[26] A. Brockhinke, J. Krüger, M. Heusing, M. Letzgus, Measurement and simulation of rotationally-resolved chemiluminescence spectra in flames, Appl. Phys. B 107 (2012) 539-549.

[27] M. Köhler, A. Brockhinke, M. Braun-Unkhoff, K. Kohse-Höinghaus, Quantitative laser diagnostic and modeling Study of C_2 and CH chemistry in combustion, J. Phys. Chem. A 114 (2010) 4719-4734.

[28] D. Alviso, M. Mendieta, J. Molina, J.C. Rolón, Flame imaging reconstruction method using high resolution spectra data of OH*, CH*, and C_2* radicals, Int. J. Thermal Sciences 121 (2017) 228-236.

[29] N. Docquier, S. Belhalfaoui, F. Lacas, N. Darabiha, C. Rolón, Experimental and numerical study of chemiluminescence in methane/air high-pressure flames for active control applications, Proc. Combust. Inst. 28 (2000) 1765-1774.

[30] A. Hossain, Y. Nakamura, A numerical study on the ability to predict the heat release rate using CH* chemiluminescence in non-sooting counterflow diffusion flames, Combust. Flame 161 (2014) 162-172.

[31] S. Karanani, D. Dunn-Rankin, Visualizing CH* chemiluminescence in sooting flames, Combust. Flame 160 (2013) 2275-2278.

[32] T. Kathrotia, M. Fikri, M. Bozkurt, M. Hartmann, U. Riedel, C. Schulz, Study of the H+M reaction forming OH*: kinetics of OH* chemiluminescence in hydrogen combustion systems, Combust. Flame 157 (2010) 1261-1273.

[33] I.S. Zaslonko, S.M. Kogarko, E.B. Mozzhukin, Y.P. Petrov, Thermal decomposition of nitromethane in shock waves, Kinet. Catal. 13 (1972) 1001-1005.

[34]] H. Dong, W. Yong-Guo, L. Hong-Bing, S. Zhu-Mei, Studies on high speed reaction spectrum of nitromethane under high temperature and high pressure. Chin. J. High Press. Phys. 8 (1994) 296-301.

[35] S.L. Sheehe, S.I. Jackson, Spatial Distribution of Spectrally Emitting Species in a Nitromethane-Air Diffusion Flame and Comparison with Kinetic Models, *in submission*

[36] R.W.B. Pearse, A.G. Gaydon, The identification of molecular spectra, 4th ed., Chapman and Hall, U.K., 1974.

[37] J.A. Vanderhoff, Spectral studies of propellant combustion: experimental details and emission results for M-30 propellant, Memorandum Report BRL-MR-3714 (1988), Aberdeen Proving Ground, Maryland, USA.

[38] J.A. Vanderhoff, Species profiles in solid propellant flames using absorption and emission spectroscopy, Combust. Flame 84 (1991) 73-92

[39] H. Reisler, M. Mangir, C. Wittig, The kinetics of free radicals generated by IR laser photolysis, I. Reactions of $C_2(a^3\Pi_u)$ with NO, vinyl cyanide, and ethylene, J. Chem. Phys. 71 (5) (1973) 2109-2117.

[40] S. Zabarnick, Laser-Induced Diagnostics and Chemical Kinetic Modeling of a $CH_4/NO_2/O_2$ Flame at 55 torr, Combust. Flame 85 (1991) 27-50

[41] K.P. Huber, G. Herzberg, Constants of diatomic molecules, NIST Chemistry WebBook, NIST Standard Reference Database Number 69, Eds. P.J. Linstrom, W.G. Mallard, National Institute of Standards and Technology, Gaithersburg MD, 20899, doi:10.18434/T4D303, (retrieved April 2018).

[42] J.K. Cashion, J.C. Polyani, Infrared chemiluminescence from the gaseous reaction atomic H. plus NO: HNO in emission, J. Chem. Phys. 30 (1959) 317-318.

[43] M.J.Y. Clement, D.A. Ramsay, Predissociation in the HNO molecule, Can. J. Phys. 39 (1961) 205-209.

[44] F.W. Dalby, The spectrum and structure of the HNO molecule, Can. J. Phys. 36 (1958) 1336-1371.

[45] P.F. Bernath, Spectra of atoms and Molecules, Oxford University Press, New York, 1995.

[46] I.E. Gordon, L.S. Rothman, C. Hill, R.V. Kochanov, Y. Tan, P.F. Bernath, M. Birk, V. Boudon, A. Campargue, K.V. Chance, B.J. Drouin, J.-M. Flaud, R.R. Gamache, J.T. Hodges, D. Jacquemart, V.I. Perevalov, A. Perrin, K.P. Shine, M.-A.H. Smith, J. Tennyson, G.C. Toon, H. Tran, V.G. Tyuterev, A. Barbe, A.G. Császár, V.M. Devi, T. Furtenbacher, J.J. Harrison, J.-M. Hartmann, A. Jolly, T.J. Johnson, T. Karman, I. Kleiner, A.A. Kyuberis, J. Loos, O.M. Lyulin, S.T. Massie, S.N. Mikhailenko, N. Moazzen-Ahmadi, H.S.P. Müller, O.V. Naumenko, A.V. Nikitin, O.L. Polyansky, M. Rey, M. Rotger, S.W. Sharpe, K. Sung, E. Starikova, S.A. Tashkun, J. Vander Auwera, G. Wagner, J. Wilzewski, P. Wcisło, S. Yu, E.J. Zak, The HITRAN2016 Molecular Spectroscopic Database, J. Quant. Spectrosc. Radiat. Transf. (2017) 203, 3-69. doi:10.1016/j.jqsrt.2017.06.038.]

[47] A. Fontijn, C.B. Meyer, H.I. Schiff, Absolute quantum yield measurements of the NO-O reaction and its use as a standard for chemiluminescent reactions, J. Chem. Phys. 40 (1) (1964) 64-70.

[48] D.E. Paulsen, W.F. Sheridan, R.E. Huffman, Thermal and recombination Emission of NO_2, J. Chem. Phys. 53 (2) (1970) 647-658.

[49] K.H. Becker, W. Groth, D. Thran, The mechanism of the air-afterglow NO+O → $NO_2 + h\nu$, Chem. Phys. Lett. 15 (2) (1972) 215-220.

[50] D. Golomb, N.W. Rosenberg, C. Aharonian, Oxygen atom determination in the upper atmosphere by chemiluminescence of nitric oxide, J. Geophysical Research 70 (5) (1965) 1155-1173.

[51] K. Honma, O. Kajimoto, Crossed beam study of the reaction of van der Waals molecule $O+(NO)_2 \rightarrow NO_2^* + NO$, J. Chem. Phys. 86 (10) (1987) 5491-5499.

[52] A. Delon, R. Jost, Laser induced dispersed fluorescence spectra of jet cooled NO_2: the complete set of vibrational levels up to 10 000 cm^{-1} and the onset of the X^2A_1 – $A\ ^2B_2$ vibronic interaction, J. Chem. Phys. 95 (1991) 5686-5700

[53] R. Jost, M. Joyeux, M. Jacon, The X^2A_1 – A^2B_2 conical intersection in NO_2: determination of the coupling parameter λ from high-resolution experimental data, Chem. Phys. 283 (2002) 17-28

[54] M.A.A. Clyne, B.A. Thrush, Mechanism of chemiluminescent reactions Involving nitric oxide—the H+NO reaction, Discussion of the Faraday Society 33 (1962) 139-148.

[55] T. Ishiwata, H. Akimoto, I. Tanaka, Chemiluminescent spectra of HNO and DNO in the reaction of $O(^3P)/O_2$ with NO and hydrocarbons or aldehydes, Chem. Phys. Lett. 21 (2) (1973) 322-325.

[56] T. Ishiwata, H. Akiomoto, I. Tanaka, Chemiluminescence of HNO sensitized by $O_2(^1\Delta_g)$ in the reaction systems of $O(^3P) + C_3H_6 + NO + O_2(^1\Delta_g)/O_2$ and $H+NO+O_2(^1\Delta_g)/O_2$, Chem. Phys. Lett. 27 (2) (1974) 260-263.

[57] N. Washida, H. Akimoto, M. Okuda, HNO formed in the H+NO+M reaction system, J. Phys. Chem. 82 (21) (1978) 2293-2299.

[58] Y. Yoshimura, H. Ohyama, T. Hamada, T. Kasai, K. Kuwata, The internal energy distribution of HNO ($\tilde{A}^2A''$) formed in the reaction of H+NO, Chem. Phys. Lett. 106 (4) (1984) 271-275.

[59] K. Honma, O. Kajimoto, Crossed-beam study of the reaction of the van der Waals molecule $H+(NO)_2$, J. Chem. Phys. 92 (1990) 1657-60.

[60] R.S. Lewis, K.Y. Tang, E. K.C. Lee, Photoexcited chemiluminescence spectroscopy: Detection of hydrogen atoms produced from single vibronic level photolysis of formaldehyde $(\tilde{A}^1A_2)^*$, J. Chem. Phys. 65(7) (1976) 2910-2911

[61] R. Guadagnini, G.C. Schatz, S.P. Walch, Global potential energy surfaces for the lowest $^1A'$, $^3A'$, and $^1A''$ states of HNO, J. Chem. Phys. 102 (2) (1995) 774- 783.

[62] C.K. Law, Combustion Physics, Cambridge University Press, New York, 2006.

[63] V. Weiser, N. Eisenreich, Fast Emission Spectroscopy for a Better Understanding of Pyrotechnic Combustion behavior, Propellants, Explosives, Pyrotechnics, 30 (1) (2005) 67-78

[64] D. Sun, G. Lu, H. Zhou, Y. Yan, Measurement of Soot Temperature, Emissivity and Concentration of a Heavy-Oil Flame through Pyrometric Imaging, 2012 Instrument and Measurement Technology Conference, IEEE, Graz, Austria (2012), doi: https://doi.org/10.1109/I2MTC.2012.6229499

[65] A. Delon, R. Jost, Laser induced dispersed fluorescence spectra of jet cooled NO_2: the complete set of vibrational levels up to 10 000 cm^{-1} and the onset of the $X^2A_1 - A\ ^2B_2$ vibronic interaction, J. Chem. Phys. 95 (1991) 5686-5700

[66] R. Jost, M. Joyeux, M. Jacon, The $X^2A_1 - A^2B_2$ conical intersection in NO_2: determination of the coupling parameter λ from high-resolution experimental data, Chem. Phys. 283 (2002) 17-28